



# UNIVERSITÀ DI PARMA

## ARCHIVIO DELLA RICERCA

University of Parma Research Repository

Designing a functional type 2 copper center that has nitrite reductase activity within  $\alpha$ -helical coiled coils

This is the peer reviewed version of the following article:

*Original*

Designing a functional type 2 copper center that has nitrite reductase activity within  $\alpha$ -helical coiled coils / Tegoni, M., Fangting, Y.u., Manuela, B., James E., P.H., Vincent L., P.. - In: PROCEEDINGS OF THE NATIONAL ACADEMY OF SCIENCES OF THE UNITED STATES OF AMERICA. - ISSN 0027-8424. - 109:52(2012), pp. 21234-21239. [10.1073/pnas.1212893110]

*Availability:*

This version is available at: 11381/2605649 since: 2015-12-11T11:49:29Z

*Publisher:*

*Published*

DOI:10.1073/pnas.1212893110

*Terms of use:*

Anyone can freely access the full text of works made available as "Open Access". Works made available

*Publisher copyright*

note finali coverpage

(Article begins on next page)

# Designing a functional type 2 copper center that has nitrite reductase activity within $\alpha$ -helical coiled coils

Matteo Tegoni<sup>a</sup>, Fangting Yu<sup>b</sup>, Manuela Bersellini<sup>a</sup>, James E. Penner-Hahn<sup>b,c</sup>, and Vincent L. Pecoraro<sup>b,1</sup>

<sup>a</sup>Department of Chemistry, University of Parma, 43124 Parma, Italy; and Departments of <sup>b</sup>Chemistry and <sup>c</sup>Biophysics, University of Michigan, Ann Arbor, MI 48109

Edited by Harry B. Gray, California Institute of Technology, Pasadena, CA, and approved November 12, 2012 (received for review July 26, 2012)

One of the ultimate objectives of *de novo* protein design is to realize systems capable of catalyzing redox reactions on substrates. This goal is challenging as redox-active proteins require design considerations for both the reduced and oxidized states of the protein. In this paper, we describe the spectroscopic characterization and catalytic activity of a *de novo* designed metalloprotein Cu(I/II)(TRIL23H)<sub>3</sub><sup>+2+</sup>, where Cu(I/II) is embedded in  $\alpha$ -helical coiled coils, as a model for the Cu<sub>T2</sub> center of copper nitrite reductase. In Cu(I/II)(TRIL23H)<sub>3</sub><sup>+2+</sup>, Cu(I) is coordinated to three histidines, as indicated by X-ray absorption data, and Cu(II) to three histidines and one or two water molecules. Both ions are bound in the interior of the three-stranded coiled coils with affinities that range from nano- to micromolar [Cu(II)], and picomolar [Cu(I)]. The Cu(His)<sub>3</sub> active site is characterized in both oxidation states, revealing similarities to the Cu<sub>T2</sub> center in the natural enzyme. The species Cu(II)(TRIL23H)<sub>3</sub><sup>2+</sup> in aqueous solution can be reduced to Cu(I)(TRIL23H)<sub>3</sub><sup>+</sup> using ascorbate, and reoxidized by nitrite with production of nitric oxide. At pH 5.8, with an excess of both the reductant (ascorbate) and the substrate (nitrite), the copper peptide Cu(II)(TRIL23H)<sub>3</sub><sup>2+</sup> acts as a catalyst for the reduction of nitrite with at least five turnovers and no loss of catalytic efficiency after 3.7 h. The catalytic activity, which is first order in the concentration of the peptide, also shows a pH dependence that is described and discussed.

NiR | NO | TRI peptides

Metalloproteins are involved in the most complex biomolecular processes in nature. *De novo* designed metalloproteins provide an approach for constructing metalloenzymes that reproduce the structure and function of native systems (1, 2). Three important examples of functional, *de novo* designed enzymes are the Duferrin, MID1-zinc, and zinc(II) TRI systems. The first uses Fe bound to a four-helix bundle in a redox role to oxidize phenols (3, 4), whereas the other two contain zinc(II) in a (His)<sub>3</sub> environment and are models for carbonic anhydrase (5, 6). The zinc(II) TRI system, in particular, exploits Zn(II) to mimic very well the active site structure and CO<sub>2</sub>-hydrolytic chemistry of the native enzyme, using three-stranded coiled coils (6). Among *de novo* designed systems, those containing redox active metal centers are most challenging as one must account for the coordination environment in two distinct oxidation levels.

Copper enzymes are extraordinarily efficient molecular tools carrying out many reactions, including biological denitrification (7–9), in which anaerobic bacteria use nitrogen oxide species as terminal electron acceptors in place of dioxygen. This pathway is crucial for returning fixed nitrogen to the atmosphere, thereby completing the terrestrial nitrogen cycle (7–9). Copper nitrite reductase [NiR; *Achromobacter cycloclastes* (AciNiR) or *Alcaligenes xylosoxidans* (AxNiR) among the most studied] is a homotrimeric metalloenzyme that contains both type 1 and type 2 copper sites, carrying out dissimilatory reduction of nitrite to nitric oxide (7, 8, 10, 11). The type 2 copper, at which the catalytic conversion of nitrite into nitric oxide occurs (NO<sub>2</sub><sup>-</sup> + e<sup>-</sup> + 2H<sup>+</sup> = NO + H<sub>2</sub>O), is coordinated to three imidazoles and a water molecule, forming a distorted tetrahedral environment (12). The electron necessary for the reduction of nitrite is provided by the type 1 copper (10).

Examples of Cu(I) (13, 14) and Cu(II) *de novo* designed helix bundles have been reported (15–24). However, only a few examples of controlled binding of copper at (His)<sub>3</sub> sites are known (17, 20, 21). Although Cu(I)/(II) redox processes were presented for a few systems (13, 14, 22), none was fully characterized in both oxidation states, which is essential for catalytic copper redox protein designs. We felt that Cu(TRIL23H)<sub>3</sub><sup>+2+</sup> [TRIL23H = (Ac-G[LKALEEK]<sub>3</sub>[HKALEEK]G-NH<sub>2</sub>)] was an ideal system to cycle between Cu(I) and Cu(II), because an X-ray crystal structure of Zn(II) bound to three histidines in the related peptide Hg<sub>5</sub>Zn<sub>N</sub>(CSL9CL23H)<sub>3</sub><sup>+</sup> was known (Fig. 1) (6), which suggests that the histidine residues might bind to Cu(I) in a way similar to that found in Zn(II). Herein, we explore the reactivity of both Cu(I)(TRIL23H)<sub>3</sub><sup>+</sup> and Cu(II)(TRIL23H)<sub>3</sub><sup>2+</sup> metalloproteins as NiR models and demonstrate that these systems are the most effective artificial systems for catalytic nitrite reduction in aqueous solution.

## Results

**Characterization of Cu(I) and Cu(II) Sites.** In the pH range 6–7.4, only two singlets (~7.0 and 7.7 ppm) are observed in D<sub>2</sub>O for apo-(TRIL23H)<sub>3</sub>, corresponding to the three equivalent His H<sub>δ</sub> and H<sub>ε</sub> protons, respectively. The addition of 1 eq of [Cu(I)(CH<sub>3</sub>CN)<sub>4</sub>]BF<sub>4</sub> to apo-(TRIL23H)<sub>3</sub> at pH 6 or pH 7.4 leads to changes in the NMR spectra with the appearance of multiple peaks in the range 6.6–8.7 ppm (Fig. S1 A–D). Although the spectra at these two pH values are different, possibly because of a slight change of the geometry of the (His)<sub>3</sub> site, they prove the Cu(I) coordination to the imidazole nitrogens. The presence of multiple peaks in the spectra of Cu(I)(TRIL23H)<sub>3</sub><sup>+</sup> is likely the result of the presence of different similar energy conformations at the Cu(I)(His)<sub>3</sub> site, an observation consistent with what was observed for the Cu(I) adduct of the 1–42 fragment of  $\beta$ -amyloid (25). Importantly, given the 1:1 Cu(I):(TRIL23H)<sub>3</sub> stoichiometry of these experiments, the formation of two-stranded Cu(I)(TRIL23H)<sub>2</sub><sup>+</sup> is ruled out by the absence of residual signals for the apo-peptide. The pH-<sup>1</sup>H NMR titration of equimolar Cu(I) and (TRIL23H)<sub>3</sub> solutions carried out between pH 2.27 and 7.3 showed that resonances for uncomplexed imidazole are present only up to pH 4.45 (Fig. S1 E and F). Above this pH, only Cu(I)(TRIL23H)<sub>3</sub><sup>+</sup> is present, which is consistent with a Cu(I)(His)<sub>3</sub> site.

The X-ray absorption spectroscopy edge region of Cu(I) complexes frequently shows a resolved transition at ~8,984 eV attributed to a 1s→4p transition; this is very intense for two-coordinate Cu(I), moderately intense for three-coordinate Cu(I), and almost undetectable for four-coordinate Cu(I) (26). The X-ray absorption near-edge structure (XANES) data for Cu(I)

Author contributions: M.T., F.Y., and V.L.P. designed research; M.T., F.Y., and M.B. performed research; M.T., F.Y., and J.E.P.-H. analyzed data; and M.T., F.Y., and V.L.P. wrote the paper.

The authors declare no conflict of interest.

This article is a PNAS Direct Submission.

<sup>1</sup>To whom correspondence should be addressed. E-mail: vlpec@umich.edu.

This article contains supporting information online at [www.pnas.org/lookup/suppl/doi:10.1073/pnas.1212893110/-DCSupplemental](http://www.pnas.org/lookup/suppl/doi:10.1073/pnas.1212893110/-DCSupplemental).

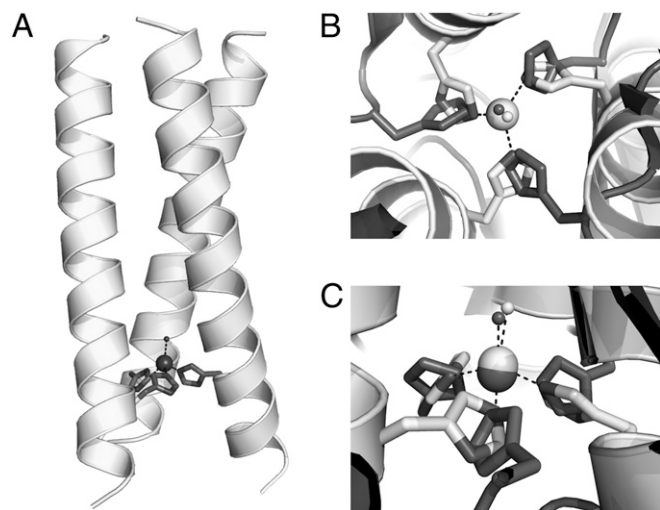


**Fig. 1.** (A) Representation of the model of the metalloprotein  $\text{Cu(II)(TRIL23H)}_3^{2+}$  based on the structure of  $\text{Hg(II)}_5[\text{Zn(II)}_N(\text{H}_2\text{O})](\text{CSL9CL23H})_3^+$  [PDB ID code 3PBJ (6)]. (B) View of the  $\text{Zn(II)(H}_2\text{O)(His)}_3$  site along the pseudo-three-fold axis of  $\text{Hg(II)}_5[\text{Zn(II)}_N(\text{H}_2\text{O})](\text{CSL9CL23H})_3^+$  (light gray), overimposed to the type 2  $\text{Cu(II)(H}_2\text{O)(His)}_3$  site in *R. sphaeroides* NiR (PDB ID code 2DY2, dark gray). Light gray for  $\text{Zn(II)(H}_2\text{O)}$ , dark gray for  $\text{Cu(II)(H}_2\text{O)}$ . Coordinated water molecules are reported as spheres. (C) Side view of the two metal sites, as in B.

$(\text{TRIL2WL23H})_3$  (Fig. S24) show a resolved  $1s \rightarrow 4p$  transition at  $\sim 8,984$  eV, characteristic of three-coordinate complexes (27). The spectra for  $\text{Cu(I)(TRIL2WL23H)}_3$  at pH 5.9 and 7.4 are indistinguishable, demonstrating that the Cu(I) structure is independent of pH over this range. The extended X-ray absorption fine structure (EXAFS) spectra for  $\text{Cu(I)(TRIL2WL23H)}_3$  (Fig. S2B and C) show peaks for both nearest-neighbor scattering and outer-shell scattering characteristic of imidazole ligation. The nearest-neighbor scattering has an amplitude consistent with three low-Z ligands, with an apparent Cu-(N/O) distance of 1.93 Å, as expected for a three-coordinate Cu(I) site. The nearest-neighbor and outer-shell scatterings are well modeled by using three imidazoles modeled as rigid groups with only a variable Cu-N distance and Debye-Waller factors proportional to those calculated ab initio (28). Inclusion of an additional shell to model a putative water ligand did not improve the fit. This, together with the XANES evidence for a three-coordinate Cu(I) and the relatively short Cu-N distance, all point to a Cu(I) that is ligated only to the three histidine ligands. The fitted Debye-Waller factor for the Cu-N shell is large ( $\sim 9 \times 10^{-3} \text{ \AA}^2$ ), suggesting that the site is distorted, as is often seen for three-coordinate Cu(I) sites. Assuming that the dynamic Debye-Waller factor is  $\sim 4 \times 10^{-3} \text{ \AA}^2$ , as seen in model compounds, the observed value implies a spread in distances of  $\sim 0.1\text{--}0.15$  Å (Table S1).

We next characterized the  $\text{Cu(II)(TRIL23H)}_3^{2+}$  using visible spectroscopy. From pH 5.8–7.4, a broad absorption maximum at 640 nm ( $\epsilon^{640 \text{ nm}} = 133\text{--}138 \text{ M}^{-1} \text{ cm}^{-1}$ ) assigned to Cu(II)  $d\text{--}d$  transitions is observed (Table S2). Similarly,  $\text{Cu(II)(TRIL2WL23H)}_3^{2+}$  presents similar molar absorbance values in the same pH range (Table S2). The absorption maxima are consistent, for both peptides, with a  $\text{Cu(II)(His)}_3$  site that might contain either one or two exogenous water ligands (predicted  $\lambda_{\text{max}}$  of  $634 \pm 11$  nm) (29). These observations prove the existence of the  $\text{Cu(II)(His)}_3$  site in this pH region and eliminate a  $\text{Cu(II)(His)}_2$  site for which a  $\lambda_{\text{max}} \sim 690$  nm is expected (29).

The EPR spectra of both  $\text{Cu(II)(TRIL23H)}_3^{2+}$  and  $\text{Cu(II)(TRIL2WL23H)}_3^{2+}$  have features typical of type 2 copper centers (Fig. S3), and for the latter, the spectra do not change significantly in the pH range 5.19–7.80. The observed  $g$  values ( $g_{\parallel} = 2.27$ ) and

hyperfine coupling constant ( $A_{\parallel} = 186$  G and 188 G for the two peptides, respectively) are somewhat larger than those observed for NiR in which a  $\text{Cu(His)}_3(\text{OH})_2$  site is present (10, 30). These parameters are more consistent with a five-coordinate structure  $\text{Cu(His)}_3(\text{OH})_2$  (31, 32), with a distorted square pyramidal geometry containing three quasi-in-plane imidazoles, as suggested by the observed  $d\text{--}d$  transition at 640 nm. Upon addition of nitrite (27 eq) to  $\text{Cu(II)(TRIL23H)}_3^{2+}$ , a 9-G decrease of the  $A_{\parallel}$  from 186 to 177 G, was observed (Fig. S3), whereas no further changes were observed for addition of nitrite up to 212 eq. Interestingly, a similar 13-G decrease in the  $A_{\parallel}$  was observed for *Rhodobacter sphaeroides* NiR upon addition and binding of nitrite, supporting the hypothesis of the direct binding of nitrite to the copper center in  $\text{Cu(II)(TRIL23H)}_3^{2+}$  (10).

**Cu(I) and Cu(II) Binding Affinities.** Metalloenzyme redox cycling is required for nitrite reduction. Based on the Nernst equation, the reduction potential can be estimated by determining the binding affinities of Cu(I) and Cu(II) to the peptide. The affinity ( $K_d$ ) of apo- $(\text{TRIL2WL23H})_3$  for Cu(II) was determined by a spectrofluorimetric titration of the apo-peptide with  $\text{CuCl}_2$ , which resulted in the quenching of the Trp fluorescence [ $K_d = 40$  (8) and 8.7 (1.1) nM at pH 5.9 and 7.4, respectively] (Fig. S4). The titration was also carried out using  $\text{Cu(NO}_3)_2$  to evaluate the role of anions in the binding of Cu(II) to  $(\text{TRIL2WL23H})_3$ , resulting in a  $K_d$  of 2.0 (3)  $\mu\text{M}$  at pH 5.9 and 6.4 (1.9) nM at pH 7.4. The dissociation constants for  $\text{Cu(I)(TRIL2WL23H)}_3^+$  were determined by visible competitive titrations using bathocuproine disulfonate as the competing ligand for Cu(I) ( $K_d = 3.1$  (7) and 0.20 (6) pM at pH 5.9 and 7.4, respectively; Fig. S4) (33). The calculated reduction potential for  $\text{Cu(II)(TRIL2WL23H)}_3^{2+}$  at pH 5.9 is 400 (30) mV using  $\text{Cl}^-$  as an anion and 500 (30) mV using  $\text{NO}_3^-$  as an anion. At pH 7.4, the potential is 430 (30) mV for both anions.

The reduction of  $\text{Cu(II)(TRIL23H)}_3^{2+}$  by addition of a stoichiometric amount (1 eq, 0.5 mol) of ascorbate can be obtained within the mixing time (Fig. 24). Although samples of  $\text{Cu(II)(TRIL23H)}_3^{2+}$  reduced with sodium ascorbate did not undergo reoxidation for 24 h when stored in a sealed cuvette, the visible band at 640 nm reappeared after the solutions were exposed to air.

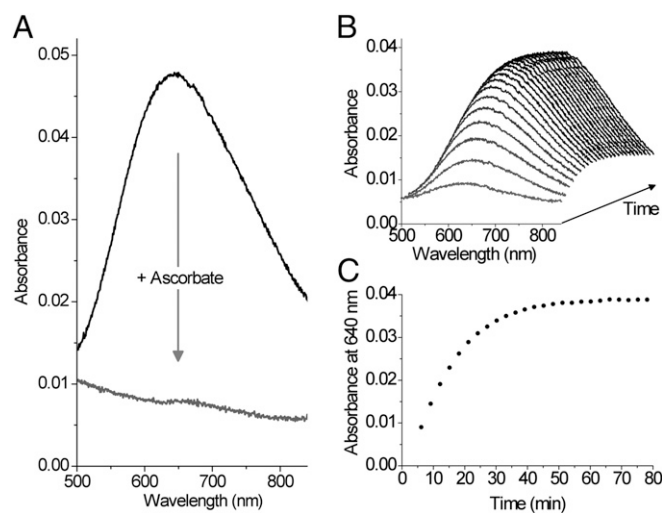


**Fig. 2.** Visible spectra of  $\text{Cu(II)(TRIL23H)}_3^{2+}$ . (A) Spectrum of a 0.34-mM solution of  $\text{Cu(II)(TRIL23H)}_3^{2+}$  in presence of 30 mM sodium nitrite in deoxygenated  $\text{H}_2\text{O}$  before (black line) and after (gray line) the addition of 1 eq of sodium ascorbate (200 mM buffer MES, pH 5.8). (B) Recovery of  $\text{Cu(II)(TRIL23H)}_3^{2+}$  absorbance. The spectra were collected every 3 min after ascorbate addition. (C) Absorbance values at 640 nm vs. time.

**NiR Activity.** We assessed the capability of nitrite to oxidize  $\text{Cu(I)(TRIL23H)}_3^{2+}$  generated in situ using ascorbate. The 640-nm absorbance of  $\text{Cu(II)(TRIL23H)}_3^{2+}$  increased over time in samples containing a 100-fold excess of nitrite (Fig. 2B and C). At pH 5.8, the recovery of 77% of the initial absorbance is obtained in 70 min. Although the recovery of 100% of the initial absorbance was not achieved, successive additions of ascorbate to the same sample allowed reduction–reoxidation cycles of the  $\text{Cu(II)(TRIL23H)}_3^{2+}$  sample for another three additions of reductant, with absorbance recoveries of over 65% of the initial absorbance (Fig. S5).

The production of NO by reacting  $\text{Cu(I)(TRIL23H)}_3^+$  with 1 eq of nitrite at pH 5.8 was demonstrated by visible spectroscopy by trapping the evolved gas as the colored  $[\text{Fe(NO)(EDTA)}]^{2-}$  complex (Fig. S6) (34). More importantly, the production of NO was observed at pH 5.8 using both  $\text{Cu(I)(TRIL23H)}_3^+$  and ascorbate-reduced  $\text{Cu(II)(TRIL23H)}_3^{2+}$ . For these two samples, the amount of trapped NO is 71% and 48% after 1 h, respectively, of that from a control sample containing  $[\text{Cu(I)(CH}_3\text{CN)}_4]^+$ .

We tested whether our system carries out NiR activity under catalytic conditions ( $C_{\text{Asc}} = 1.15$  mM,  $C_{\text{nitrite}} = 30$  mM,  $C_{\text{metallopeptide}} = 0.180$  mM). In this assay, the oxidation of ascorbate as sacrificial reductant was monitored spectrophotometrically by observing the decrease of its absorption band centered at 265 nm (Fig. 3A). The quantity of ascorbate oxidized in 175 min at pH 5.9, corrected for the background reaction, corresponds to 1.5 (2) times the moles of  $\text{Cu(II)(TRIL23H)}_3^{2+}$  and, therefore, results in a turnover number of 3.0 when expressed as moles of electrons per mole of  $\text{Cu(II)(TRIL23H)}_3^{2+}$ . Moreover, five turnovers have been measured at pH 5.8 in 220 min (Fig. 3B). The rate of the background reaction of ascorbate with nitrite is not influenced by the presence of either traces of Cu(II) ion (0.21  $\mu\text{M}$ ) or apo-(TRIL23H)<sub>3</sub> (0.90 mM, Fig. S7A), and ascorbate is stable in the absence of nitrite (Fig. S7A). The oxidation rate of the ascorbate also depends on the concentration of  $\text{Cu(II)(TRIL23H)}_3^{2+}$ , with a linear increase observed for increasing metallopeptide concentrations (0.171–0.513 mM, Fig. S7B and C). These observations suggest that ascorbate acts as a sacrificial reductant for  $\text{Cu(II)(TRIL23H)}_3^{2+}$ , and that the  $\text{Cu(I)(TRIL23H)}_3^+$  species is catalytically active in reducing nitrite to NO. Moreover, by FTIR analysis of the headspace gas, we also proved that no  $\text{N}_2\text{O}$  is produced under catalytic conditions (SI Experimental Procedures).

Both the kinetics of oxidation of  $\text{Cu(I)(TRIL23H)}_3^+$  (through the recovery of absorbance at 640 nm) and of ascorbate (through the decrease of absorbance at 265 nm) were studied as a function of pH. The initial rate of reoxidation of  $\text{Cu(I)(TRIL23H)}_3^+$  ( $v_{\text{Cu,ox}}$ ) was studied between pH 5.8 and 7.4. Although the initial increase

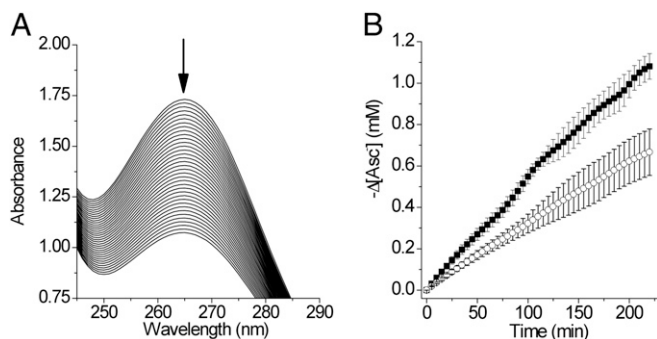


**Fig. 3.** (A) UV spectra of a solution of sodium ascorbate and sodium nitrite (pH 5.9) collected every 5 min, containing  $\text{Cu(II)(TRIL23H)}_3^{2+}$  (0.180 mM) and apo-(TRIL23H)<sub>3</sub> (0.090 mM). (B) ■, decrease of  $[\text{Asc}^-]$  vs. time in samples, as in A; ○, samples containing only apo-(TRIL23H)<sub>3</sub> (0.090 mM), pH 5.8.

**Table 1.** Pseudo-first-order rate constants for the oxidation of  $\text{Cu(I)(TRIL23H)}_3^+$  ( $k_{\text{first,Cu}}$ ) and of oxidation of ascorbate ( $k_{\text{first,Asc}}$ ) as a function of the pH ( $C_{\text{Nitrite}} = 30$  mM)

pH	$k_{\text{first,Cu}} \times 10^{-4} \text{ (s}^{-1}\text{)}$	$k_{\text{first,Asc}} \times 10^{-4} \text{ (s}^{-1}\text{)}$
5.3	—	12 (3)
5.5	—	9 (1)
5.8	5.2 (3)	4.6 (3)
5.9	—	4.40 (16)
6.0	2.8 (3)	2.4 (2)
6.5	0.65 (3)	0.68 (3)
7.0	0.22 (8)	—

of absorbance at 640 nm is large at pH 5.8, at pH 7.0 this absorption is very small and at pH 7.4 we did not observe any significant increase of absorbance in 2 h (Fig. S84). The pseudo-first-order rate constants  $k_{\text{first,Cu}}$  ( $v_{\text{Cu,ox}} = k_{\text{first,Cu}}[\text{Cu(II)(TRIL23H)}_3^{2+}]$ ) determined from the initial rates (12 min) as a function of pH are reported in Table 1 and in Fig. 4A and Fig. S8. The rate of oxidation of ascorbate in the presence of  $\text{Cu(I)(TRIL23H)}_3^+$  and nitrite ( $v_{\text{Asc,ox}}$ ) was studied in the pH range 5.3–6.5. The initial rate of the reaction  $1/2\text{Asc}^- + \text{Cu(II)(TRIL23H)}_3^{2+} = 1/2\text{dH-Asc} + \text{Cu(I)(TRIL23H)}_3^+ + 1/2\text{H}^+$  decreases with increasing pH, as shown in Fig. S8C and D (dH-Asc = dehydroascorbate). The values of the pseudo-first-order constant  $k_{\text{first,Asc}}$  ( $v_{\text{Asc,ox}} = k_{\text{first,Asc}}[\text{Cu(II)(TRIL23H)}_3^{2+}]$ ) as a function of pH are reported in Table 1 and Fig. 4.

## Discussion

Several copper complexes with nitrogen ligands as mimics for the type 2 copper site of NiR were synthesized in recent years (9, 35, 36). They have extensively expanded our understanding of the structures as well as the mechanisms of native copper NiR. Nevertheless, almost all the synthetic models are soluble only in organic solvents. The study of copper NiR itself is complicated by having two distinct copper centers with different functions and physical properties. De novo designed metallopeptides are soluble in water, can enforce lower metal coordination numbers, and inhibit dimerization reactions while providing a hydrophobic environment that contains a single metal cofactor at which the desired chemistry may be performed. In a recent study, we showed that a de novo design strategy is highly effective for providing mimics of carbonic anhydrase using a mononuclear Zn(II)-based hydrolytic system (6). In this report, we explore the more challenging objective of obtaining a de novo designed redox-based assembly that carries out a reaction similar to that at the  $\text{Cu}_{\text{T2}}$  site in NiR.

Because both Zn(II) and Cu(I) are  $d^{10}$  metals, we felt that the latter ion could be bound similarly to Zn(II) in the same (His)<sub>3</sub> site found in  $\text{Hg}_5\text{Zn}_1(\text{CSL9CL23H})_3^+$ , as recently reported (6). A comparison of this Zn(II) site to that of type 2 Cu(II) in  $\text{CuNiR}$  [*R. sphaeroides* NiR, Protein Data Bank (PDB) ID code 2DY2] is shown in Fig. 1. The overlaid metal sites show that the metal ion environments are well matched and, in both structures, the metal ions are coordinated to the imidazole  $\text{N}_\epsilon$  with a water molecule occupying the fourth coordination position, as observed in NiR.

To test this hypothesis, we subjected the  $\text{Cu}^{n+}(\text{TRIL23H})_3^{n+}$  system to multiple spectroscopic methods. Our NMR data on  $\text{Cu(I)(TRIL23H)}_3^+$  and XANES and EXAFS data on  $\text{Cu(I)(TRIL2WL23H)}_3^+$  indicate that all three histidine imidazoles are coordinated to Cu(I) above pH 4.8. These observations suggest that Cu(I) has a three-coordinate distorted trigonal planar geometry within the coiled coils. Our visible and EPR data also confirm the presence of a  $\text{Cu(II)(TRIL23H)}_3^{2+}$ , where Cu(II) has parameters for a type 2 copper center, suggesting a tris-histidine set of protein ligands. However, in NiR, Cu(II) is four-coordinate, whereas the EPR spectra of  $\text{Cu(II)(TRIL23H)}_3^{2+}$  indicate that the

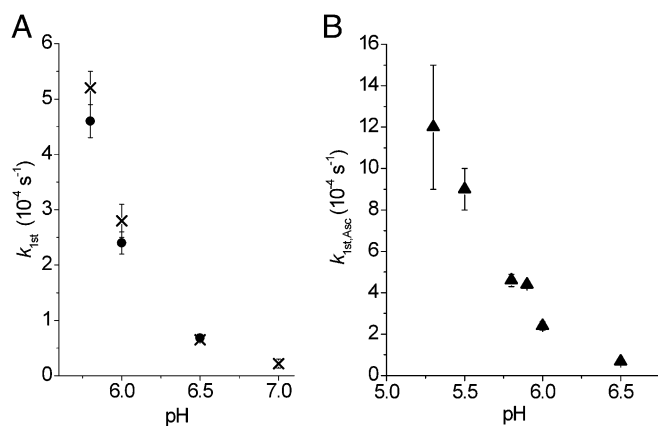


**Fig. 4.** (A) Values of  $k_{\text{fir,Cu}}$  (X) and  $k_{\text{fir,Asc}}$  (●) as a function of the pH. (B) Pseudo-first-order rate constants ( $k_{\text{fir,Asc}}$  ▲) values as a function of the pH.

center likely is five-coordinate. We also have shown that this peptide possesses a good to high affinity for both oxidation states of copper. The affinity for Cu(I) in particular, which is in the nanomolar range, is remarkably close to that found for the N-terminal fragment 1–14 of human copper transporter hCtr1, which contains three histidine residues ( $\sim 0.16 \text{ pM}$ ) (37) and much higher than that of amyloid  $\beta_{1-42}$  ( $\sim 50 \text{ nM}$ ) (38).

On the basis of these stability constants, we calculated a reduction potential for  $\text{Cu(II)(TRIL23H)}_3^{2+}$  of  $\sim 400\text{--}500 \text{ mV}$  (pH 5.9 and pH 7.4 for both chloride and nitrate as counteranions). This value is higher than those measured for type 2 copper centers in NiR, which have been reported to be 218 mV at pH 6.0 and 137 mV at pH 8.4 for *R. sphaeroides* (12), or in the range 220–310 mV at pH 7.0 for *A. cycloclastes* and *A. xylooxidans* (39). One possible explanation for this relatively high reduction potential for Cu-peptide is that Cu(I) is strongly stabilized by its distorted trigonal planar structure. In addition, the coordination number changes from three to five [as shown in the EXAFS data for Cu(I) and EPR and UV-visible data for Cu(II)], leading to the change of geometry of the site, creating a relatively large energy barrier for oxidation. In native enzymes,  $\text{Cu}_{\text{T2}}$  sites are coupled with either a  $\text{Cu}_{\text{T1}}$  site or other cofactors to function. In particular, a  $\text{Cu(His)}_3$  site is involved in electron transfer (peptidylglycine  $\alpha$ -hydroxylating monooxygenase) (40), in dioxygen activation (amine oxidase) (41), or nitrite reduction (NiR) (42). Although the potential of the  $\text{Cu}_{\text{T1}}$  sites in native proteins spans from 350 to 790 mV (43, 44), those of  $\text{Cu}_{\text{T2}}$  sites are lower. For example, the potential of  $\text{Cu}_{\text{T2}}$  site in laccase (extracted from *Rhus vernicifera*), is one of the highest (390 mV at pH 7.4), but still lower than that of our construct (45).

Although higher than those of NiRs, these reduction potentials suggested that  $\text{Cu(I)(TRIL23H)}_3^+$  would have NiR activity [formal  $E^0$  of nitrite  $\sim 1.3 \text{ V}$  at pH 6.0 (7)]. Therefore, we assessed the reactivity of  $\text{Cu(II)(TRIL23H)}_3^{2+}$  with nitrite. Because the reduction potential of ascorbate in the pH range 5–7 is  $\sim 100 \text{ mV}$ , we expected that  $\text{Cu(II)(TRIL23H)}_3^{2+}$  could be quantitatively reduced to  $\text{Cu(I)(TRIL23H)}_3^+$  by the addition of sodium ascorbate. The bleaching of the 640-nm *d-d* band occurred within the mixing time, which confirmed this prediction. Thus, a reduced metalloprotein could be formed in situ, which prompted us to investigate the NiR activity of  $\text{Cu(I)(TRIL23H)}_3^+$  by assessing the production of NO and the possibility of cycling between the Cu(II) and Cu(I) forms of the metalloprotein in the presence of  $\text{Asc}^-$  as the reductant and  $\text{NO}_2^-$  the oxidant.

The production of nitric oxide and the oxidation to the Cu(II) form of the metalloprotein may be observed by reacting  $\text{Cu(I)(TRIL23H)}_3^+$  with nitrite. It is worth mentioning that the detected NO production is expected to be less than quantitative,

as loss of NO due to system leaks and possible reactions involving NO as a radical will diminish the total amount of NO produced. However, these results demonstrate that both the oxidized metal site and NO are products of the reaction of  $\text{Cu(I)(TRIL23H)}_3^+$  with nitrite. These data in concert demonstrate that we have made a functional mimic of the NiR copper type 2 center.

The spectrophotometric data for the ascorbate oxidation reaction allowed us to establish that  $\text{Cu(II)(TRIL23H)}_3^{2+}$  undergoes five turnovers, expressed as moles of electrons per moles of Cu(II). As the reduction of Cu(II) into Cu(I) occurs within seconds after the addition of ascorbate, the turnover number of five corresponds to five nitrite ions reduced after 220 min. No catalyst decomposition is observed as the progress curve for absorbance vs. time remains in the linear regime throughout the 220-min reaction time. Hence, the turnover number is limited by the electron donor concentration rather than by the catalyst stability (Fig. 3B).

Both the rate of oxidation of ascorbate and the reoxidation of  $\text{Cu(I)(TRIL23H)}_3^+$  have been found to be pH dependent. Moreover, the rate constants for the oxidation of ascorbate by  $\text{Cu(II)(TRIL23H)}_3^{2+}$  ( $k_{\text{fir,Asc}}$ ; Table 1 and Fig. 4A) under catalytic conditions match the first-order rate constants  $k_{\text{fir,Cu}}$  for the oxidation of  $\text{Cu(I)(TRIL23H)}_3^+$  by nitrite (both  $k_{\text{fir}}$  values refer to samples containing 30 mM nitrite) reasonably well. This demonstrates that the electron transfer from  $\text{Cu(I)(TRIL23H)}_3^+$  to nitrite with the formation of  $\text{Cu(II)(TRIL23H)}_3^{2+}$  is the rate-determining step of the overall catalytic process, and rules out the possibility of ascorbate consumption by the formed NO, which should lead to the observed values for  $k_{\text{fir,Asc}}$  significantly larger than those of  $k_{\text{fir,Cu}}$ . We believe that the reasons for this pH dependence do not stand, as found for the enzyme NiR, in the deprotonation of a coordinated water molecule at the  $\text{Cu(II)(His)}_3$  site, as both the visible absorption and the EPR spectra do not show significant changes in the pH range 5.2–7.4 (Table S2, Fig. S3) (12, 46). More likely, this pH dependence is the result either of some changes at the  $\text{Cu(I)(His)}_3$  active site in that pH range [as suggested by changes in the NMR spectra of  $\text{Cu(I)(TRIL23H)}_3^+$ ] or of the involvement of  $\text{H}^+$  in the reduction step of nitrite to NO ( $\text{NO}_2^- + 2\text{H}^+ + e^- = \text{NO} + \text{H}_2\text{O}$ ).

$\text{Cu(II)(TRIL23H)}_3^{2+}$  exhibits a pseudo-first-order rate constant  $k_{\text{fir,Asc}}$  at pH 5.9 (Table 1) of  $4.40 \times 10^{-4} \text{ s}^{-1}$ , with this catalyst exhibiting five turnovers in 3.7 h (pH 5.8). Although  $\text{Cu(II)(TRIL23H)}_3^{2+}$  possesses a very low NiR activity compared with the NiR enzyme [ $\sim 1,500 \text{ s}^{-1}$  at pH 5.8 for *Alcaligenes faecalis* NiR with *Pseudoazurin* as the electron donor (46)], de novo design has provided the only example of a stable and functional  $\text{Cu(His)}_3$  site in aqueous solution, thus representing a highly advanced model of NiR. It is clear from the pH profile that higher activities can be achieved at even lower pH, although these rates are still not competitive with NiR. Numerous other mononuclear models that examine NiR reactivity have been explored so far (31, 36, 47–50). These compounds are split into those whose activities have been investigated in nonaqueous solutions (34, 49, 50) and those that have been examined in aqueous solutions (47, 48, 51–54). In the case of nonaqueous systems, the reaction rates are higher than those observed in aqueous solutions, and the ligands in some cases model the tris-His environment of NiR relatively well (9, 49, 50). Although the nonaqueous conditions allowed the number of water molecules bound to copper to be controlled, the use of these complexes does not account for several features of the NiR reaction, such as the different dielectrics between the exterior and the enzyme pocket and the hydrogen bonding that occurs in aqueous conditions. There are only a few examples of functional copper complexes that can reduce nitrite in aqueous solutions, and in general these systems have far lower rates than those observed in nonaqueous conditions. In some cases, these complexes produced  $\text{N}_2\text{O}$  rather than NO (48, 54), whereas the

systems in which multiple turnovers were observed have been associated mostly with electrocatalytic reactions, particularly heterogeneous systems (i.e., catalyst linked to the electrode surface) (47, 48, 51, 54). One example has been reported of a copper complex capable of at least four turnovers in 15 min when reduced using photoactivated  $[\text{Ru}(\text{II})(\text{bpy})_3]^{2+}$  as the electron donor, but with a significant decrease in activity (NO generation) after two turnovers (52). The present chemistry advances the field in the following ways: we provide a reasonable, although not exact, structural model for both Cu(I) and Cu(II) for NiR, which has NiR activity in aqueous solution and an almost selective production of NO. Although our rates are modest, especially compared to native enzymes, we do see multiple turnovers under homogeneous conditions, with rates that are 10 times faster than those previously observed for a homogeneous electroreduced complex [ $k_{\text{cat}} = 5.4 \times 10^{-5} \text{ s}^{-1}$  at pH 5.5 (47)]. Moreover, when the latter complex is linked to an electrode surface or photoreduced, faster rates have been observed but at the expense of the stability of the catalyst (47, 51–53). In contrast, our data reveal that our catalyst is robust and carries out multiple turnovers with no decrease in efficiency. Equally important, the product of our reaction is dominantly NO as opposed to other homogeneous catalysts, which also form  $\text{N}_2\text{O}$  (48, 54). The latter point may reflect the steric constraints and the proper matching of the coordination geometry for Cu(I) and Cu(II) in our system.

## Experimental Procedures

**General Procedures.** All samples containing Cu(I) were handled in the glove box using oxygen-free water or buffered aqueous solutions. The procedures for sample preparation, chemical compounds used, and instrumentation are given in *SI Experimental Procedures*.

**Peptide Synthesis and Purification.** TRIL23H and TRIL2W23H (Ac-GWKALEEK [LKALEEK]<sub>2</sub>HKALEEKG-NH<sub>2</sub>) were synthesized on an Applied Biosystems 433A peptide synthesizer using standard protocols (55) and purified and characterized as reported (56). Solutions of the apo-peptides were prepared by weight in doubly distilled water or in buffered solutions where appropriate.

**NMR Spectroscopy.** Samples of apo-(TRIL23H)<sub>3</sub> and Cu(I)(TRIL23H)<sub>3</sub><sup>+</sup> (2.4–5.7 mM) were prepared in deoxygenated 50 mM buffered D<sub>2</sub>O (MES or Hepes at pH 6.0 or 7.4, respectively). The <sup>1</sup>H-NMR titration of Cu(I)(TRIL23H)<sub>3</sub><sup>+</sup> (1.6 mM in 25 mM MES buffer in D<sub>2</sub>O) was performed in the pH range 7.3–2.3. A 0.1-M NaOD solution in D<sub>2</sub>O was used as the titrant.

**X-Ray Absorption Spectroscopy.** A 1-mM Cu(I)(TRIL2W23H)<sub>3</sub> solution was made in the glove box with 50 mM degassed MES buffer. Excess apo-peptide (1 mM) was added to ensure the free Cu(I) concentration was minimum (<0.01% total copper concentration). The samples were mixed with 50% glycerol as a glassing agent, loaded into a sample cell, and frozen in liquid nitrogen. Measurements were carried out at Stanford Synchrotron Radiation Lightsource (SSRL) beamline 7–3 with an Si (220) double-crystal monochromator and a flat Rh-coated harmonic rejection mirror. Samples were maintained below 10 K with an Oxford Instruments liquid helium cryostat. Data were measured as fluorescence excitation spectra using a 30-element Ge array detector normalized to incident intensity measured with an N<sub>2</sub>-filled ion chamber. Data were measured with steps of 0.25 eV in the XANES region (1 s integration time) and 0.05 Å<sup>-1</sup> in the EXAFS region to  $k = 13.5 \text{ \AA}^{-1}$  (1–20 s integration,  $k^3$  weighted). Energies were calibrated by assigning the lowest energy inflection point of a copper metal foil as 8,980.3 eV. An initial E<sub>0</sub> value of 9,000 eV was used to convert data to  $k$ -space, and the background was removed using a three-region cubic spline. EXAFS data were analyzed using EXAFSPAK (57) and FEFF 9.0 (58).

**Visible Spectroscopy.** The visible spectra of Cu(II)(TRIL23H)<sub>3</sub> (0.3 mM) at different pH were collected in the pH range 5.8–7.4 (200 mM MES buffer). The visible spectra of Cu(II)(TRIL2W23H)<sub>3</sub> (0.26 mM) at different pH conditions were collected in an unbuffered aqueous solution by adjusting the pH using small aliquots of concentrated KOH.

**Binding Constants Determination.** The affinity of (TRIL2W23H)<sub>3</sub> for Cu(I) was determined by competitive binding assay with disodium bathocuproinedisulfonate (Na<sub>2</sub>BCS) as a competitive chelator in 50 mM aqueous buffer (MES, pH 5.9; Hepes, pH 7.4) (33). The affinity of TRIL2W23H for Cu(II) was determined by monitoring the quenching of Trp fluorescence upon binding to Cu(II) in 50 mM buffered solutions (MES, pH 5.9; Hepes, pH 7.4).

**EPR Spectroscopy.** A Cu(II)(TRIL23H)<sub>3</sub><sup>2+</sup> solution (1.67 mM) in 200 mM aqueous Hepes at pH 7.4 was added with aliquots of NaNO<sub>2</sub> (1.16 M stock solution in 200 mM Hepes, pH 7.4; NO<sub>2</sub><sup>-</sup>:Cu = 0, 27, 53, and 212). Solutions of Cu(II)(TRIL2W23H)<sub>3</sub> (1 mM) were made unbuffered, using KOH/HCl to adjust pH in the range 5.19–7.80. Glycerol was added as a glassing agent. X-band EPR spectra were collected at 77 K.

**NiR Activity. NO production.** Cu(I)(TRIL23H)<sub>3</sub><sup>+</sup> solutions (2.26 mM in 200 mM aqueous MES, pH 6.0) were prepared in rubber-sealed vials and reacted with nitrite by adding an equimolar amount of NaNO<sub>2</sub>. The produced NO was stripped off through a gentle oxygen-free N<sub>2</sub> stream, and trapped in a cuvette containing [Fe(EDTA)]<sup>2-</sup> (34). The visible spectrum of the latter solution was collected after 1 h. The NO produced was quantitated from the spectrum of the obtained [Fe(NO)(EDTA)]<sup>2-</sup> solution ( $\epsilon_{432 \text{ nm}} = 780 \text{ M}^{-1} \cdot \text{cm}^{-1}$ ) (34).

**Cu(I) oxidation.** Solutions of Cu(II)(TRIL23H)<sub>3</sub><sup>2+</sup> (0.33 mM) in 200 mM aqueous MES at different pH between 5.8 and 7.4 were prepared in a rubber-sealed quartz cuvette (1-cm path length) and added with NaNO<sub>2</sub> to obtain a 30-mM nitrite concentration. The reduction of Cu(II)(TRIL23H)<sub>3</sub><sup>2+</sup> was obtained by adding 1 eq of sodium ascorbate (ascorbate:Cu = 0.5 mol ratio). The visible absorption spectra were collected every 3 min for 2 h.

**Ascorbate oxidation in presence of nitrite.** Samples containing Cu(II)(TRIL23H)<sub>3</sub><sup>2+</sup> (0.180 mM), apo-(TRIL23H)<sub>3</sub> (0.090 mM), and sodium nitrite (30 mM) were prepared in 200 mM aqueous MES buffer at different pH between 5.3 and 6.5. To initiate the reaction, sodium ascorbate was added to obtain a 1.15-mM concentration. The solutions were transferred into rubber-sealed 0.1-cm pathlength cuvettes and the UV spectra collected every 5 min for 3–4 h. All reactions were performed in triplicate.

**Detection and quantification of N<sub>2</sub>O.** A solution of 3 mL 50-mM phosphate buffer containing 0.33 mM CuCl<sub>2</sub>, 0.5 mM (TRIL2W23H)<sub>3</sub> (apo-peptide:Cu<sup>2+</sup> = 1.5:1), and 0.1 M NaNO<sub>2</sub> (300 eq wrt. Cu<sup>2+</sup>) was prepared in a 50-mL Schlenk flask under anaerobic conditions. The reaction was initiated by adding sodium ascorbate at pH 5.8 [final C<sub>Asc</sub> = 17 mM (50 eq vs. Cu<sup>2+</sup>)]. After 3.5 h, the gas in the headspace was transferred into a gas IR cell. The absorption peaks at 2,234.8 and 2,212.9 cm<sup>-1</sup> were integrated and calibrated with a series of known amounts of N<sub>2</sub>O (59, 60).

**ACKNOWLEDGMENTS.** The authors thank the National Institutes of Health (NIH) for support of this research (Grant R01 ES0 12236 to V.L.P.); the Italian Ministry of Foreign Affairs for financial support (to M.T.; Direzione Generale per la Promozione del Sistema Paese, relevant bilateral project Italy-USA 2011-12); and Consortium of Universities for Research in Chemistry of Metals in Biological Systems (CIRCMSB; Bari, Italy) for a fellowship (to M.B.). Portions of this research were carried out at SSRL, a Directorate of SLAC National Accelerator Laboratory and an Office of Science User Facility SSRL, which is operated for the US Department of Energy (DOE) Office of Science by Stanford University. The SSRL Structural Molecular Biology Program is supported by the DOE Office of Biological and Environmental Research and by the NIH, National Institute of General Medical Sciences (including P41GM103393), and the National Center for Research Resources (P41RR001209).

1. Lu Y, Yeung N, Sieracki N, Marshall NM (2009) Design of functional metalloproteins. *Nature* 460(7257):855–862.
2. Nanda V, Koder RL (2010) Designing artificial enzymes by intuition and computation. *Nat Chem* 2(1):15–24.
3. Kaplan J, DeGrado WF (2004) De novo design of catalytic proteins. *Proc Natl Acad Sci USA* 101(32):11566–11570.
4. Faiella M, et al. (2009) An artificial di-iron oxo-protein with phenol oxidase activity. *Nat Chem Biol* 5(12):882–884.

5. Der BS, Edwards DR, Kuhlman B (2012) Catalysis by a de novo zinc-mediated protein interface: Implications for natural enzyme evolution and rational enzyme engineering. *Biochemistry* 51(18):3933–3940.
6. Zastrow ML, Peacock AFA, Stuckey JA, Pecoraro VL (2012) Hydrolytic catalysis and structural stabilization in a designed metalloprotein. *Nat Chem* 4(2): 118–123.
7. Averill BA (1996) Dissimilatory nitrite and nitric oxide reductases. *Chem Rev* 96(7): 2951–2964.

8. Suzuki S, Kataoka K, Yamaguchi K (2000) Metal coordination and mechanism of multicopper nitrite reductase. *Acc Chem Res* 33(10):728–735.
9. Wasser IM, de Vries S, Moëne-Loccoz P, Schröder I, Karlin KD (2002) Nitric oxide in biological denitrification: Fe/Cu metalloenzyme and metal complex NO(x) redox chemistry. *Chem Rev* 102(4):1201–1234.
10. Olesen K, et al. (1998) Spectroscopic, kinetic, and electrochemical characterization of heterologously expressed wild-type and mutant forms of copper-containing nitrite reductase from *Rhodobacter sphaeroides* 2.4.3. *Biochemistry* 37(17):6086–6094.
11. Merkle AC, Lehnert N (2012) Binding and activation of nitrite and nitric oxide by copper nitrite reductase and corresponding model complexes. *Dalton Trans* 41(12):3355–3368.
12. Jacobson F, et al. (2007) pH dependence of copper geometry, reduction potential, and nitrite affinity in nitrite reductase. *J Biol Chem* 282(9):6347–6355.
13. Hong J, et al. (2006) Evidence that a miniature CuI metalloprotein undergoes collisional electron transfer in the inverted Marcus region. *Angew Chem Int Ed Engl* 45(37):6137–6140.
14. Hong J, Kharenko OA, Ogawa MY (2006) Incorporating electron-transfer functionality into synthetic metalloproteins from the bottom-up. *Inorg Chem* 45(25):9974–9984.
15. Xie F, Sutherland DEK, Stillman MJ, Ogawa MY (2010) Cu(I) binding properties of a designed metalloprotein. *J Inorg Biochem* 104(3):261–267.
16. Schnepf R, et al. (2001) De novo design and characterization of copper centers in synthetic four-helix-bundle proteins. *J Am Chem Soc* 123(10):2186–2195.
17. Tanaka T, et al. (2004) Two-metal ion, Ni(II) and Cu(II), binding  $\alpha$ -helical coiled coil peptide. *J Am Chem Soc* 126(43):14023–14028.
18. Schnepf R, Haehnel W, Wieghardt K, Hildebrandt P (2004) Spectroscopic identification of different types of copper centers generated in synthetic four-helix bundle proteins. *J Am Chem Soc* 126(44):14389–14399.
19. Shiga D, et al. (2009) The effect of the side chain length of Asp and Glu on coordination structure of Cu(2+) in a de novo designed protein. *Biopolymers* 91(11):907–916.
20. Kiyokawa T, et al. (2004) Binding of Cu(II) or Zn(II) in a de novo designed triple-stranded  $\alpha$ -helical coiled-coil toward a prototype for a metalloenzyme. *J Pept Res* 63(4):347–353.
21. Ghadiri MR, Case MA (1993) De novo design of a novel heterodinuclear three-helix bundle metalloprotein. *Angew Chem Int Ed Engl* 32(11):1594–1597.
22. Shiga D, et al. (2010) Creation of a type 1 blue copper site within a de novo coiled-coil protein scaffold. *J Am Chem Soc* 132(51):18191–18198.
23. Murase S, Ishino S, Ishino Y, Tanaka T (2012) Control of enzyme reaction by a designed metal-ion-dependent  $\alpha$ -helical coiled-coil protein. *J Biol Inorg Chem* 17(5):791–799.
24. Shiga D, et al. (2012) Creation of a binuclear purple copper site within a de novo coiled-coil protein. *Biochemistry* 51(40):7901–7907.
25. Raffa DF, Rickard GA, Rauk A (2007) Ab initio modelling of the structure and redox behaviour of copper(I) bound to a His-His model peptide: Relevance to the  $\beta$ -amyloid peptide of Alzheimer's disease. *J Biol Inorg Chem* 12(2):147–164.
26. Kau LS, Spira-Solomon DJ, Penner-Hahn JE, Hodgson KO, Solomon EI (1987) X-ray absorption edge determination of the oxidation state and coordination number of copper. Application to the type 3 site in *Rhus vernicifera* laccase and its reaction with oxygen. *J Am Chem Soc* 109(21):6433–6442.
27. Chen K, Yuldashewa S, Penner-Hahn JE, O'Halloran TV (2003) An atypical linear Cu(I)-S2 center constitutes the high-affinity metal-sensing site in the CueR metalloregulatory protein. *J Am Chem Soc* 125(40):12088–12089.
28. Dimakis N, Bunker G (2002) Group-fitted ab initio single- and multiple-scattering EXAFS Debye-Waller factors. *Phys Rev B Condens Matter* 65(20):201103.
29. Prenesti E, Daniele PG, Principe M, Ostacoli G (1999) Spectrum-structure correlation for visible absorption spectra of copper(II) complexes in aqueous solution. *Polyhedron* 18(25):3233–3241.
30. Fittipaldi M, Wijma HJ, Verbeet MP, Canters GW, Huber M (2006) Electronic structure of the two copper sites in nitrite reductase by 9 and 95 GHz EPR on cavity mutants. *Appl Magn Reson* 30(3):417–426.
31. Kujime M, Izumi C, Tomura M, Hada M, Fujii H (2008) Effect of a tridentate ligand on the structure, electronic structure, and reactivity of the copper(I) nitrite complex: Role of the conserved three-histidine ligand environment of the type-2 copper site in copper-containing nitrite reductases. *J Am Chem Soc* 130(19):6088–6098.
32. Nairn AK, et al. (2006) (N-Benzyl-bis-N',N''-saliicylidene)-cis-1,3,5-triaminocyclohexane copper(II): A novel catalyst for the aerobic oxidation of benzyl alcohol. *Dalton Trans* (1):172–176.
33. Xiao Z, Loughlin F, George GN, Howlett GJ, Wedd AG (2004) C-terminal domain of the membrane copper transporter Ctr1 from *Saccharomyces cerevisiae* binds four Cu(I) ions as a cuprous-thiolate polynuclear cluster: Sub-femtomolar Cu(I) affinity of three proteins involved in copper trafficking. *J Am Chem Soc* 126(10):3081–3090.
34. Monzani E, et al. (2000) Binding of nitrite and its reductive activation to nitric oxide at biomimetic copper centers. *J Biol Inorg Chem* 5(2):251–261.
35. Tolman WB (2006) Using synthetic chemistry to understand copper protein active sites: A personal perspective. *J Biol Inorg Chem* 11(3):261–271.
36. Richards RL, Durrant MC (2002) Copper complexes with N-donor ligands as models of the active centres of nitrite reductase and related enzymes. *J Chem Res* 2002(3):95–98.
37. Haas KL, Putterman AB, White DR, Thiele DJ, Franz KJ (2011) Model peptides provide new insights into the role of histidine residues as potential ligands in human cellular copper acquisition via Ctr1. *J Am Chem Soc* 133(12):4427–4437.
38. Alies B, Badei B, Faller P, Hureau C (2012) Reevaluation of copper(I) affinity for amyloid- $\beta$  peptides by competition with ferrozine—an unusual copper(I) indicator. *Chemistry* 18(4):1161–1167.
39. Suzuki S, et al. (1997) Spectroscopic characterization and intramolecular electron transfer processes of native and type 2 Cu-depleted nitrite reductases. *J Biol Inorg Chem* 2(2):265–274.
40. Blackburn NJ, Rhames FC, Ralle M, Jaron S (2000) Major changes in copper coordination accompany reduction of peptidylglycine monooxygenase: Implications for electron transfer and the catalytic mechanism. *J Biol Inorg Chem* 5(3):341–353.
41. Wilmot CM (2003) Oxygen activation in a copper-containing amine oxidase. *Biochem Soc Trans* 31(Pt 3):493–496.
42. Libby E, Averill BA (1992) Evidence that the type 2 copper centers are the site of nitrite reduction by *Achromobacter cycloclastes* nitrite reductase. *Biochem Biophys Res Commun* 187(3):1529–1535.
43. Ghosh S, et al. (2009) Thermodynamic equilibrium between blue and green copper sites and the role of the protein in controlling function. *Proc Natl Acad Sci USA* 106(13):4969–4974.
44. Solomon EI, Sundaram UM, Machonkin TE (1996) Multicopper oxidases and oxygenases. *Chem Rev* 96(7):2563–2606.
45. Reinhammar BRM, Vänngård TI (1971) The electron-accepting sites in *Rhus vernicifera* laccase as studied by anaerobic oxidation-reduction titrations. *Eur J Biochem* 18(4):463–468.
46. Wijma HJ, Jeuken LJC, Verbeet MP, Armstrong FA, Canters GW (2006) A random-sequential mechanism for nitrite binding and active site reduction in copper-containing nitrite reductase. *J Biol Chem* 281(24):16340–16346.
47. Isoda N, Yokoyama H, Nojiri M, Suzuki S, Yamaguchi K (2010) Electroreduction of nitrite to nitrogen oxide by a copper-containing nitrite reductase model complex incorporated into collagen film. *Bioelectrochemistry* 77(2):82–88.
48. Komeda N, et al. (1995) Molecular structure of nitro- and nitrito-copper complexes as reaction intermediates in electrochemical reduction of nitrite to dinitrogen oxide. *Bull Chem Soc Jpn* 68(2):581–589.
49. Kujime M, Fujii H (2006) Spectroscopic characterization of reaction intermediates in a model for copper nitrite reductase. *Angew Chem Int Ed Engl* 45(7):1089–1092.
50. Woollard-Shore JG, Holland JP, Jones MW, Dilworth JR (2010) Nitrite reduction by copper complexes. *Dalton Trans* 39(6):1576–1585.
51. Hiratsu T, Suzuki S, Yamaguchi K (2005) Electroreduction of nitrite on gold electrode modified with Cu-containing nitrite reductase model complex. *Chem Commun (Camb)* (36):4534–4535.
52. Yamaguchi K, Okada T, Suzuki S (2006) Photochemical reduction of nitrite catalyzed by a Cu-containing nitrite reductase model complex and a photosensitizer under irradiation with visible light. *Inorg Chem Commun* 9(10):989–991.
53. Migita Y, et al. (2009) Electrocatalytic nitrite reduction to nitrogen oxide by a synthetic analogue of the active site of Cu-containing nitrite reductase incorporated in Nafion film. *Electroanalysis* 21(22):2441–2446.
54. Nagao H, Komeda N, Mukaida M, Suzuki M, Tanaka K (1996) Structural and electrochemical comparison of copper(II) complexes with tripodal ligands. *Inorg Chem* 35(23):6809–6815.
55. Chang WC, White PD (2000) *Fmoc Solid Phase Peptide Synthesis: A Practical Approach*, eds Chang WC, White PD (Oxford Univ Press, New York).
56. Farrer BT, Harris NP, Balchus KE, Pecoraro VL (2001) Thermodynamic model for the stabilization of trigonal thiolato mercury(II) in designed three-stranded coiled coils. *Biochemistry* 40(48):14696–14705.
57. George GN (2000) EXAFSPAK. SSRL, Stanford University, USA. Available at <http://ssrl.slac.stanford.edu/exafspak.html>.
58. Ankudinov AL, Rehr JJ (1997) Relativistic calculations of spin-dependent x-ray absorption spectra. *Phys Rev B Condens Matter* 56(4):R1712–R1716.
59. Xu N, Campbell ALO, Powell DR, Khandogin J, Richter-Addo GB (2009) A stable hyponitrite-bridged iron porphyrin complex. *J Am Chem Soc* 131(7):2460–2461.
60. Kagann RH (1982) Infrared absorption intensities for N2O. *J Mol Spectrosc* 95(2):297–305.

# Supporting Information

Tegoni et al. 10.1073/pnas.1212893110

## SI Experimental Procedures

**General Procedures.** All samples containing Cu(I) were handled in the glove box using oxygen-free water or buffered aqueous solutions obtained by sparging them with an oxygen-free nitrogen stream for 6 h. The stock solution of  $[\text{Cu}(\text{CH}_3\text{CN})_4]\text{BF}_4$  was prepared in degassed acetonitrile ( $\sim 0.13$  M). Unless otherwise stated, all  $\text{Cu(I)}(\text{TRIL23H})_3^+$  or  $\text{Cu(II)}(\text{TRIL23H})_3^{2+}$  solutions were prepared by reacting apo-( $\text{TRIL23H})_3$  in aqueous solution with stoichiometric amounts of  $[\text{Cu}(\text{CH}_3\text{CN})_4]\text{BF}_4$  acetonitrile solution or  $\text{CuCl}_2$  aqueous solution.  $^1\text{H}$  NMR spectra were collected on a Varian MR400 spectrometer using gastight tubes where appropriate. The pH values were registered using Hamilton glass microelectrodes. The pH values in  $\text{D}_2\text{O}$  were corrected using the formula reported in the literature (1).  $[\text{Cu}(\text{CH}_3\text{CN})_4]\text{BF}_4$  was purchased by Sigma-Aldrich, dissolved in degassed acetonitrile to obtain a stock solution  $\sim 0.13$  M, and standardized by spectrophotometric titrations using 2,9-dimethyl-1,10-phenanthroline (2). IR spectra were collected on a Perkin-Elmer Spectrum BX FTIR spectrometer, using an NaCl window gas IR cell. UV-visible spectra were collected on a Varian Cary 100 UV-Vis spectrophotometer provided with a thermostat device, using matched quartz cells of 1 and 0.1 cm path length. EPR spectra were collected on a Bruker EMX X-band EPR spectrometer provided with a liquid nitrogen cryostat. Fluorescence spectra were collected on a Fluoromax-2 fluorimeter.

**X-ray absorption data analysis procedure.** Single- and multiple-scattering fittings of extended X-ray absorption fine structure (EXAFS) data were performed using EXAFSPAK (3) with ab initio amplitude and phase parameters calculated using FEFF 9.0 (4). X-ray absorption near-edge structure (XANES) data were normalized using EXAFSPAK. An initial model of  $\text{Cu(I)}$ -imidazole coordination was built based on the averaged bond distances reported for the crystal structures of synthetic molecules containing  $\text{Cu(I)}$ -imidazole constituent.

**Binding constants determination.** The affinity of the  $(\text{His})_3$  site in the three-stranded coiled coils for  $\text{Cu(I)}$  and  $\text{Cu(II)}$  was determined using the peptide  $\text{TRIL2WL23H}$ , with a Leu substituted by Trp at position 2 of  $\text{TRIL23H}$  as a spectroscopic tag for concentration determination purposes (5). The concentration of peptide stock solution was determined from Trp absorbance at 280 nm (5). A solution of 40  $\mu\text{M}$   $\text{Cu(I)}$  and 80  $\mu\text{M}$   $(\text{TRIL2WL23H})_3$  was prepared in the glove box in aqueous 50 mM buffer (MES, pH 5.9; HEPES, pH 7.4) and titrated with bathocuproine disulfonate ( $\text{BCS}^{2-}$ , 5 mM stock solution, final  $C_{\text{BCS}}:C_{\text{Cu(I)}} = 3.7$ ). The formation of  $[\text{Cu}(\text{BCS})_2]^{3-}$  was monitored by visible spectroscopy ( $\lambda_{\text{max}} = 483$  nm;  $\epsilon^{483 \text{ nm}} = 13,300 \text{ M}^{-1}\cdot\text{cm}^{-1}$ ;  $\log \beta_2 = 19.8$ ) (6). The absorbance at 483 nm increased as  $\text{BCS}^{2-}$  was titrated into the  $\text{Cu(I)}$ -peptide solution. All titrant additions were carried out in the glove box. Specfit32 was used to fit the spectrophotometric data, taking into account the protonation equilibrium of  $\text{BCS}^{2-}$  at pH 5.9 (7).

A 500–800-nM solution of  $(\text{TRIL2WL23H})_3$  in 50 mM aqueous buffer (MES, pH 5.9; HEPES, pH 7.4) was titrated with 486  $\mu\text{M}$   $\text{CuCl}_2$  solution, which was diluted from a 0.0486-M  $\text{CuCl}_2$  solution, the concentration of which was confirmed by inductively coupled plasma optical emission spectroscopy. Upon each addition, the solution was stirred for 10 min to reach equilibrium and the fluorescence spectra were recorded. The apo-( $\text{TRIL2WL23H})_3$  was titrated with the  $\text{CuCl}_2$  solution up to  $\text{Cu(II)}:\text{apo-(TRIL2WL23H)}_3 = 3$ . The affinity constants were obtained by treating the fluorescence spectra with Specfit32 (7), taking into account the formation of the  $\text{Cu(II)}$ /HEPES 1:1 complex ( $\log \beta = 3.22$ ) (8).

The formal redox potential for the couple  $\text{Cu(II)}/\text{Cu(I)}$  ( $\text{TRIL2WL23H})_3^{2+/+}$  ( $E^0_{\text{Pep}}$ ) was calculated through the equation  $E^0_{\text{Pep}} = E^0_{\text{Cu(II/I)}} + 0.0591 \cdot \lg(K_d^{\text{Cu(II)}}/K_d^{\text{Cu(I)}})$ , where  $K_d$  is the dissociation constants (affinities) of the  $\text{Cu(II)}$  and  $\text{Cu(I)}$  metalloptides, and  $E^0_{\text{Cu(II/I)}}$  the standard reduction potential for the couple  $\text{Cu(II/I)}$ .

**Reactivity with Ascorbate. Reduction of  $\text{Cu(II)}(\text{TRIL23H})_3^{2+}$  by ascorbate.** The in situ reduction of  $\text{Cu(II)}(\text{TRIL23H})_3^{2+}$  into  $\text{Cu(I)}(\text{TRIL23H})_3^+$  was monitored by addition of sodium ascorbate (0.565  $\mu\text{mol}$ , 1 eq) to a 0.34-mM  $\text{Cu(II)}(\text{TRIL23H})_3^{2+}$  solution in deoxygenated 200-mM MES buffer (pH 6.0) obtained in 3 mL in a rubber-sealed quartz cuvette. The spectra were collected before and after ascorbate addition.

**Nitrite reductase activity. NO production.**  $\text{NaNO}_2$  stock solutions ( $\sim 0.5$  mM) were prepared in 200 mM aqueous MES, pH 6.0, and added to the copper/peptide solution using a gastight syringe. A 0.01-M  $[\text{Fe}(\text{EDTA})]^{2-}$  solution was prepared from  $\text{FeSO}_4 \cdot 7\text{H}_2\text{O}$  and  $\text{H}_2\text{EDTA}$  in deoxygenated 1-M citrate aqueous buffer at pH 5.0. The latter solution (3 mL) was put in a rubber-sealed quartz cuvette, the spectrum was registered, and then the cuvette was connected to the reaction vial through a steel canula and kept in an ice bath at 0 °C throughout the entire experiment. The reaction in the first solution was initiated by adding  $1.13 \times 10^{-3}$  mmol of  $\text{NaNO}_2$  (1 eq, from a 58.6-mM solution in 200 mM MES, pH 6.0) to the copper/peptide solution, using a gastight syringe. The NO produced was quantified from the difference spectrum [ $\epsilon_{432 \text{ nm}} = 780 \text{ M}^{-1}\cdot\text{cm}^{-1}$  for  $(\text{Fe}[\text{NO}][\text{EDTA}])^{2-}$ ] (9).

The control reaction was performed using an aqueous solution of  $[\text{Cu}(\text{CH}_3\text{CN})_4]\text{BF}_4$ , at the same conditions described above. The production of NO starting from  $\text{Cu(II)}(\text{TRIL23H})_3^{2+}$  reduced in situ with ascorbate was performed using the same condition described above (200 mM MES, pH 6.0).  $\text{CuCl}_2 \cdot 2\text{H}_2\text{O}$  (1.13 mmol,  $\sim 0.07$  M in water) was added to the peptide, followed by sodium ascorbate (0.565 mmol). All solutions were prepared in a glove box.

**Ascorbate oxidation in presence of nitrite.** The turnover number (expressed as equivalents of electrons per equivalents of copper ions) for the oxidation reaction of ascorbate by nitrite in presence of  $\text{Cu(II)}(\text{TRIL23H})_3^{2+}$  as the catalyst was determined by UV spectroscopy at pH 5.9, monitoring the change in the absorbance of the ascorbate band at 265 nm. The variation of the concentration of ascorbate over time was calculated using the molar absorbance of ascorbate reported in the literature, taking into account the effective pH and a  $\text{p}K_a$  of ascorbic acid of 4.02. A 2.4-mL solution containing  $(\text{TRIL23H})_3$  (0.30 mM) and sodium nitrite (31.6 mM) was prepared in the glove box using a degassed 200-mM MES solution in water. The pH was corrected to the desired value (5.8 or 5.9) by adding small aliquots of a concentrated KOH solution in degassed water. Aliquots ( $\sim 380$   $\mu\text{L}$ ) of this solution were added with 20  $\mu\text{L}$  of a  $\text{Cu(II)}$  chloride solution ( $\sim 3.8$  mM) to obtain samples containing  $\text{Cu(II)}$  (0.180 mM),  $(\text{TRIL23H})_3$  (0.270 mM), and sodium nitrite (30 mM). The reaction of oxidation of ascorbate was started in the glove box by injecting  $\sim 20$   $\mu\text{L}$  of a freshly prepared solution of sodium ascorbate in degassed water (21 mM) to obtain a final ascorbate concentration of  $\sim 1.15$  mM [corresponding to a 6.4-fold excess with respect to  $\text{Cu(II)}$ ]. The solution was transferred into a rubber-sealed 0.1-cm path-length cuvette, and the UV spectrum (240–290 nm) collected every 5 min for 3–5 h total reaction time. The first spectrum was collected  $\sim 10$  min after ascorbate addition. The control samples containing only apo-peptide were

prepared as reported above using a 90- $\mu\text{M}$  peptide solution, by adding degassed water in place of the Cu(II) solution. This concentration corresponds to the excess of apo-peptide in the samples containing Cu(II)(TRIL23H) $_3^{2+}$ . The oxidation reaction in presence or absence of Cu(II) was monitored in triplicates. The turnover number (equivalent of electrons per moles of copper) was calculated as two times the average moles of ascorbate consumed in the sample containing Cu(II)(TRIL23H) $_3^{2+}$  subtracted by the moles of ascorbate consumed in the sample containing apo-(TRIL23H) $_3^{2+}$  divided by the moles of Cu(II). Additional control samples containing sodium nitrite (30 mM) in presence or absence of copper chloride (0.21  $\mu\text{M}$ ) added with sodium ascorbate (final concentration  $\sim 1.15$  mM) were prepared in a way similar to the one described above, and their spectra (240–290 nm) collected in triplicate every 5 min for 60 min. A 0.21- $\mu\text{M}$  concentration of Cu(II) is  $\sim 1.5$  times the calculated amount of free Cu(II) at pH 5.9 in a sample containing the fully oxidized form of the peptide and a 50% excess of apo-peptide, based on the determined stability constants. The control of the stability of ascorbate in absence of nitrite was established by preparing samples containing Cu(II) (0.180 mM), (TRIL23H) $_3$  (0.270 mM), and sodium ascorbate (1.15 mM).

The rate of oxidation of ascorbate and the pseudo-first-order rate constants were calculated as described in *SI Experimental Procedures, Calculations*. The dependence of the reaction rate on the concentration of Cu(II)(TRIL23H) $_3^{2+}$  was studied in the 0.171–0.513-mM metalloprotein concentration. All samples contained a 0.5-eq excess of apo-peptide. Both samples and controls have been prepared as described above, and all contained 30 mM nitrite and  $\sim 1.15$  mM ascorbate. The control samples also contained a 0.085–0.257-mM apo-peptide corresponding to the excess of apo-peptide in the related metalloprotein samples. The spectra in the 240–290-nm range were collected every 3 min, and the samples run in triplicate. The pH dependence of the rate of oxidation of ascorbate in presence of Cu(II)(TRIL23H) $_3^{2+}$  was studied in the pH interval 5.3–6.5. The samples, prepared as described above, contained 0.180 mM copper chloride and 0.270 mM (TRIL23H) $_3$  (corresponding to a 0.180-mM Cu(II)(TRIL23H) $_3^{2+}$  and a 0.090-mM excess of apo-peptide), 30 mM sodium nitrite, and  $\sim 1.15$  mM sodium ascorbate. All samples were prepared in 200 mM MES buffer solution in water, and the pH was checked before adding the freshly prepared sodium ascorbate solution to initiate the reaction. The control samples all contained 0.090 mM apo-peptide, 30 mM nitrite, and  $\sim 1.15$  mM ascorbate.

**Detection of N<sub>2</sub>O.** A reaction mixture of 0.33 mM Cu(II)(TRIL2WL23H) $_3$  with 0.17-mM excess of apo-(TRIL2WL23H) $_3$  and 0.1 M NaNO<sub>2</sub> was prepared in the glove box with 50 mM phosphate buffer at pH 5.8 in a Schlenk flask. The reaction was initiated by injecting a stock solution of sodium ascorbate, preadjusted to pH 5.8. The final concentration of sodium ascorbate in the solution was 0.017 M. Control reaction was set up with 0.17 mM apo-(TRIL2WL23H) $_3$ , and all the other conditions were kept the same. The gas IR cell (10 cm, NaCl window) was vacuumed before connecting to the reaction flask. The IR spectra were collected on a Perkin-Elmer FTIR Spectrum BX instrument. Henry's law was used to calculate the distribution of the putative production of N<sub>2</sub>O in aqueous and gaseous phase. The Henry constant for N<sub>2</sub>O/water at room temperature was calculated based on ref. 10. A calibration curve was made by diluting a series of N<sub>2</sub>O-saturated 50-mM phosphate buffer solution into the same reaction setup with the same headspace volume. The system was equilibrated for 1 h before connecting to the gas IR cell, and FTIR data were collected. The absorption peaks at 2,234.8 and 2,212.9 cm<sup>-1</sup> were integrated. Based on the Beer–Lambert law, 3.30  $\times 10^{-8}$  mol N<sub>2</sub>O was produced after 3.5 h, which is 0.09% of the amount of NO produced. Taking into account the instrument error, as well as pipetting errors during the dilution, we con-

clude that essentially no N<sub>2</sub>O was produced by the catalytic reaction during the process.

**Calculations.** The initial rates of oxidation of Cu(I)(TRIL23H) $_3^+$  in presence of nitrite ( $v_{\text{Cu,ox}}$ ) were determined by monitoring the increase of absorbance of the  $d-d$  band at 640 nm. The rate of oxidation of copper has been calculated taking into account the absorbance values at 640 nm in the first 12 min after the collection of the first spectrum. The analysis of the absorption data ensured the linearity of the data as a function of time. The  $v_{\text{Cu,ox}}$  has been calculated as  $v_{\text{Cu,ox}} = \Delta C_{\text{Cu(II)(TRIL23H)}_3^{2+}} / \Delta t$  and expressed as molar  $\times$  seconds<sup>-1</sup>. In this equation,  $\Delta C_{\text{Cu(II)(TRIL23H)}_3^{2+}} = (A^{640 \text{ nm}} - A_0^{640 \text{ nm}}) / (\epsilon_{\text{Cu}} \cdot d)$ , where  $A^{640 \text{ nm}}$  is the absorbance at a given time  $t$ ,  $A_0^{640 \text{ nm}}$  the absorbance of the first collected spectrum (3 min after ascorbate addition),  $\epsilon_{\text{Cu}}$  the molar absorbance of Cu(II)(TRIL23H) $_3^{2+}$  at the given pH and at 640 nm, and  $d$  the path length (1 cm). The molar absorbance  $\epsilon_{\text{Cu}}$  has been established using the absorbance at 640 nm of the spectrum of the sample registered before adding ascorbate by the Cu(II)(TRIL23H) $_3^{2+}$  concentration. The  $\epsilon_{\text{Cu}}$  ranged from 133 to 139 M<sup>-1</sup>·cm<sup>-1</sup> from pH 5.8 to pH 7.0. The  $v_{\text{Cu,ox}}$  values, as the slope of  $(A^{640 \text{ nm}} - A_0^{640 \text{ nm}}) / (\epsilon_{\text{Cu}} \cdot d)$  as a function of time, were calculated by linear least-squares regression using the SPSS program (11). No background reaction (reoxidation of copper) has been observed in absence of nitrite after injection of ascorbate within a few hours. The first-order rate constants ( $k_{\text{first,Cu}}$ ;  $v_{\text{Cu,ox}} = k_{\text{first,Cu}} \cdot [\text{Cu(II)(TRIL23H)}_3^{2+}]$ ) were obtained by dividing the determined  $v_{\text{Cu,ox}}$  rates by the Cu(II)(TRIL23H) $_3^{2+}$  concentration.

The initial rate of oxidation of ascorbate ( $v_{\text{Asc,ox}}$ ) for the reaction  $1/2\text{Asc}^- + \text{Cu(II)(TRIL23H)}_3^{2+} = 1/2\text{dH-Asc} + \text{Cu(I)(TRIL23H)}_3^+ + 1/2\text{H}^+$  has been determined by monitoring the decrease of absorbance of ascorbate at 265 nm (dH-Asc = dehydroascorbate). All reactions were performed in triplicate. The dependence of the reaction rate on the concentration of Cu(II)(TRIL23H) $_3^{2+}$  (0.171–0.513 mM) was studied at pH 5.9. The turnover numbers have been calculated using the moles of ascorbate oxidized in the Cu(II)(TRIL23H) $_3^{2+}$  sample, corrected by the background reaction, monitoring the reactions for 3–5 h at pH 5.8 or 5.9. The turnover numbers, expressed as equivalents of electrons per equivalents of copper ions, were obtained by dividing the moles of ascorbate oxidized (after 220 min at pH 5.8, after 175 min at pH 5.9) by the moles of Cu(II)(TRIL23H) $_3^{2+}$ , and multiplying this value by two (ascorbate as two electron donor).

The rate of ascorbate oxidation has been calculated taking into account the absorbance values at 265 nm in the first 25 min after the collection of the first spectrum. The analysis of the absorption data ensured the linearity of the data as a function of time. The  $v_{\text{Asc,ox}}$  has been calculated as  $v_{\text{Asc,ox}} = -2\Delta C_{\text{Asc}} / \Delta t$  and expressed as molar  $\times$  minutes<sup>-1</sup> [ $1/2\text{Asc}^- + \text{Cu(II)(TRIL23H)}_3^{2+} = 1/2\text{dH-Asc} + \text{Cu(I)(TRIL23H)}_3^+ + 1/2\text{H}^+$ ]. In this equation,  $\Delta C_{\text{Asc}} = (A^{265 \text{ nm}} - A_0^{265 \text{ nm}}) / (\epsilon_{\text{Asc}} \cdot d)$ , where  $A^{265 \text{ nm}}$  is the absorbance at a given time  $t$ ,  $A_0^{265 \text{ nm}}$  the absorbance of the first collected spectrum (usually  $\sim 10$  min after ascorbate addition),  $\epsilon_{\text{Asc}}$  the molar absorbance of ascorbate at the given pH and at 265 nm, and  $d$  the path length (0.1 cm). The molar absorbance  $\epsilon_{\text{Asc}}$  has been established taking into account the molar absorption of protonated and deprotonated ascorbate (12), their molar fractions as calculated by the Hyss program (13) for a 1.15-mM ascorbate concentration, and a  $pK_a$  of 4.02. The  $\epsilon_{\text{Asc}}$  ranged from 13,959 to 14,524 M<sup>-1</sup>·cm<sup>-1</sup> from pH 5.3 to pH 6.5. The  $v_{\text{Asc,ox}}$  values, as the slope of  $2 \times (A^{265 \text{ nm}} - A_0^{265 \text{ nm}}) / (\epsilon_{\text{Asc}} \cdot d)$  values as a function of time, were calculated by linear least-squares regression using the SPSS program (11). All  $v_{\text{Asc,ox}}$  values were corrected for the background reaction  $1/2\text{Asc}^- + \text{NO}_2^- + 2\text{H}^+ = 1/2\text{dH-Asc} + \text{NO} + \text{H}_2\text{O}$  by subtracting the rates of ascorbate oxidation as determined for the proper control solutions. The first-order









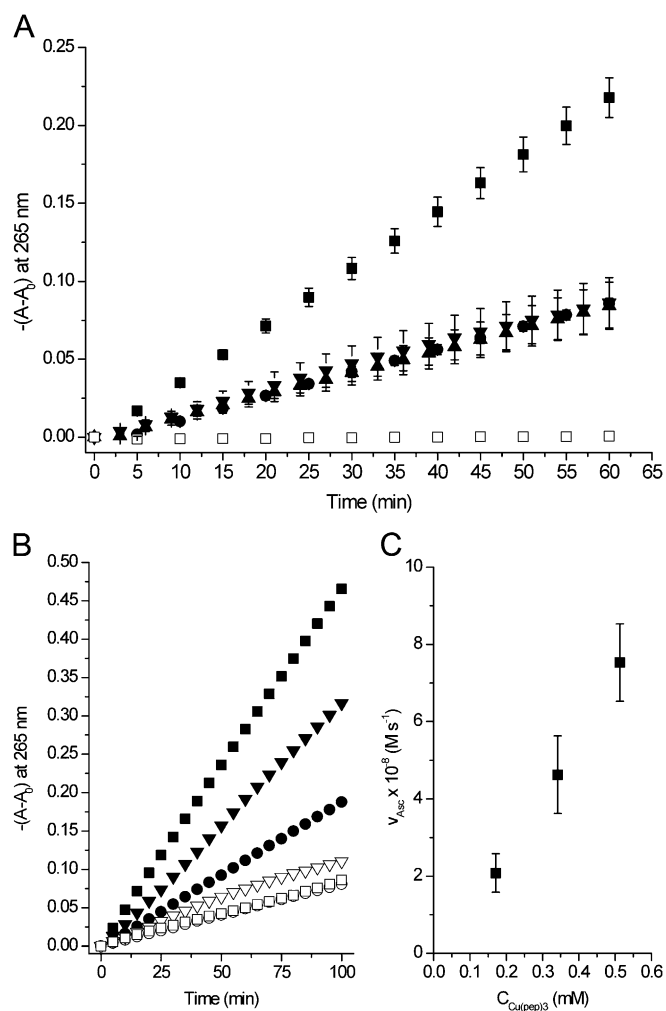


**Fig. S7.** (A) Values of  $-(A-A_0)$  at 265 nm vs. time for solutions of sodium ascorbate (1.15 mM) and sodium nitrite (30 mM) in deoxygenated aqueous 200-mM MES buffer at pH 5.9, containing  $\text{Cu(II)(TRIL23H)}_3^{2+}$  (0.180 mM) (■), apo-(TRIL23H)<sub>3</sub> (90 μM) (●), Cu(II) chloride (0.21 μM) (▲), or only ascorbate and nitrite (▼). □, sodium ascorbate (1.15 mM) and Cu(II)(TRIL23H)<sub>3</sub><sup>2+</sup> (0.180 mM) in deoxygenated 200-mM MES buffer at pH 5.9. (B) Values of  $-(A-A_0)$  at 265 nm as a function of time for solutions of sodium ascorbate (1.15 mM) and sodium nitrite (30 mM) in deoxygenated aqueous 200-mM MES buffer at pH 5.9 for increasing concentrations of Cu(II)(TRIL23H)<sub>3</sub><sup>2+</sup> [Cu(pep)<sub>3</sub>]. ■, 0.171 mM; ▲, 0.342 mM; ●, 0.513 mM [or apo-(TRIL23H)<sub>3</sub> □, 86 μM; ▽, 171 μM; ○, 257 μM]. (C) Rate constants ( $V_{\text{ascr}}$ ) for the Cu(II)(TRIL23H)<sub>3</sub><sup>2+</sup>-catalyzed reaction as a function of the concentration of the metalloprotein.



**Table S1. EXAFS data simulation parameters**

First shell			Outer shells		
Shell (X)	R(Å)	$\sigma^2(\text{Å}^2)$	Shell (Y)	R(Å)	$\sigma^2(\text{Å}^2)$
Cu(II)(TRIL2WL23H) <sub>3</sub> pH 5.9 3 imid	F = 0.408 × 10 <sup>2</sup> 1.93	E <sub>0</sub> = -10.88 0.009	3Cu-C <sup>(1)</sup> (imid)	2.92	0.013
			3Cu-C <sup>(2)</sup> (imid)	2.95	0.013
			3Cu-N <sup>(2)</sup> (imid)	4.06	0.018
			3Cu-C <sup>(3)</sup> (imid)	4.07	0.018
Cu(II)(TRIL2WL23H) <sub>3</sub> pH 5.9 3 imid 1 water	F = 0.408 × 10 <sup>2</sup> 1.93 1.81	E <sub>0</sub> = -12.20 0.009 0.037	3Cu-C <sup>(1)</sup> (imid)	2.91	0.014
			3Cu-C <sup>(2)</sup> (imid)	2.94	0.014
			3Cu-N <sup>(2)</sup> (imid)	4.05	0.019
			3Cu-C <sup>(3)</sup> (imid)	4.06	0.019
Cu(II)(TRIL2WL23H) <sub>3</sub> pH 7.4 3 imid	F = 0.349 × 10 <sup>2</sup> 1.93	E <sub>0</sub> = -10.62 0.009	3Cu-C <sup>(1)</sup> (imid)	2.92	0.014
			3Cu-C <sup>(2)</sup> (imid)	2.96	0.014
			3Cu-N <sup>(2)</sup> (imid)	4.07	0.019
			3Cu-C <sup>(3)</sup> (imid)	4.08	0.019

E<sub>0</sub>, threshold (k = 0) energy shift in eV; F, goodness of the fit: sum of the squares of the differences between experimental and calculated curves; imid, imidazole;  $\sigma^2$ , Debye-Waller factors; R, absorber-backscatterer distance; X, nearest-neighbour scatterings; Y, outer-shell scatterings.

**Table S2. Molar absorbance values (M<sup>-1</sup>·cm<sup>-1</sup>) for the Cu(II)(TRIL23H)<sub>3</sub><sup>2+</sup> and the Cu(II)(TRIL2WL23H)<sub>3</sub><sup>2+</sup> metalloptides in aqueous solution at different pH**

pH	Cu(II)(TRIL23H) <sub>3</sub> <sup>2+</sup>	Cu(II)(TRIL2WL23H) <sub>3</sub> <sup>2+</sup>
5.68	—	131
5.80	134	—
5.89	—	133
6.0	137	—
6.07	—	137
6.50	139	—
6.53	—	136
6.93	—	140
7.00	138	—
7.26	—	135
7.40	133	—
7.47	—	134